Macromolecules

pubs.acs.org/Macromolecules Article

Breaking Symmetry Rules Enhance the Options for Stereoselective Propene Polymerization Catalysis

Claudio De Rosa, Rocco Di Girolamo, Ana B. Muñoz-García, Michele Pavone, and Giovanni Talarico*

Cite This: https://dx.doi.org/10.1021/acs.macromol.0c00280 Read Online

ACCESS | Metrics & More | Article Recommendations | Supporting Information

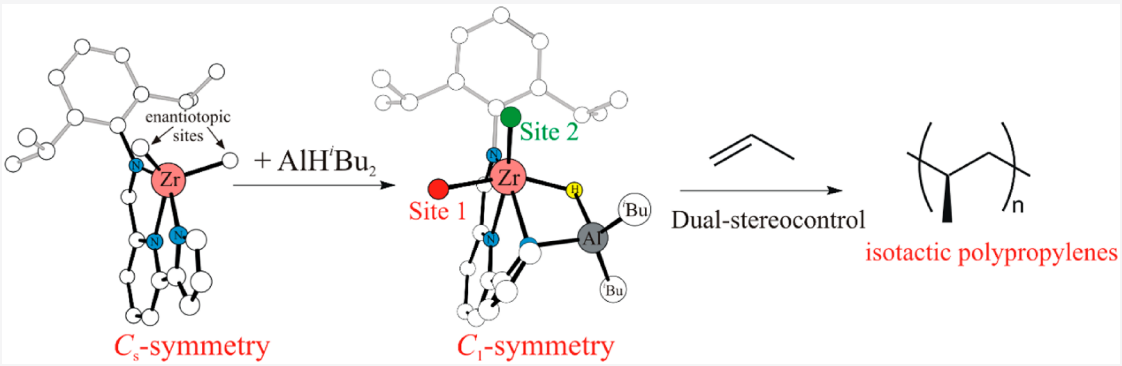

ABSTRACT: An example of breaking "Ewen's symmetry rule" for olefin catalysis polymerization is proposed by DFT calculations. Catalyst precursors with C_s symmetry are suggested to promote the isotactic propene polymerization by a modification of the active site geometry obtained via coordination with AlH−alkyl species in solution. The origin of stereocontrol in olefin polymerization is due to a dual mechanism dictated by the chiral catalyst. These findings may expand the toolbox for promoting stereoselective olefin polymerization by transition metal catalysts.

INTRODUCTION

Homogeneous transition metal (TM) catalysis for stereoselective propene polymerization is showing an extraordinary vitality despite its age.[1,2] Highly stereoregular polypropylenes (PP), both isotactic (iPP) and syndiotactic (sPP), are available,[3] due to the enantiomorphic site (ES) control where the ligand chirality selects the enantioface of the prochiral monomer.[4] Fine tuning of PP microstructure is achieved with homogeneous catalysts operating by ES mechanisms following "Ewen's symmetry rules".[5] These relationships correlate the chirality and symmetry of the catalyst precursors with the PP tacticity rationalizing the experimental evidence that C_2 (and/or C_1) and C_s symmetry precursors produce iPP and sPP, respectively (the complete list of the five classes are reported in Figure S1 of the Supporting Information).[6,7] The discovery of pentacoordinated-pyridyl−amide complexes,[8] a family of catalysts used in industrial process,[9] appeared to be an exception to these rules because ES-controlled iPP was obtained with catalysts derived from achiral C_s-symmetric precursors (such as **1** in Chart 1).[10−12] However, computational[13] and experimental studies[14,15] revealed that the active species are formed by in situ ligand modification via monomer insertion into the Hf−C_{aryl} bond, rescuing the above Ewen symmetry rules. Theoretical studies[16,17] combined with experimental techniques[18] have also ascribed the origin of stereocontrol for such pyridyl−amide systems to a direct ligand−monomer interaction instead of the usual chiral control by the growing chain.[19−22] Modifications of the pentacoordinated ligand with *N*-heteroarylpyridylamido tridentate ligands (see systems **2a** and **2b** in Chart 1) were reported by Pellecchia[23−25] and extensive high-throughput optimization of thiazole-amido hafnium compounds (see system **3**, Chart 1) was done by Symyx.[26] Interestingly, system **2a** produces iPP by ES control despite the "time averaged" C_s-symmetric structure in solution (see Figure S2).[23] The reason for this behavior is still unclear whereas more straightforward results are reported for the system **2b**[24] and **3**.[26] The latter systems (both having a C_1-symmetry) show high stereoselectivities in the propene polymerization in line with expectations (see Chart 1). As we will report in this work, the explanation for the stereoselectivity promoted by systems **2a** enlightened by DFT calculations (see Supporting Information for computational details) may be extended to system **2b** and **3** and will

Received: February 4, 2020
Revised: March 21, 2020

Chart 1. Systems Analyzed in This Study

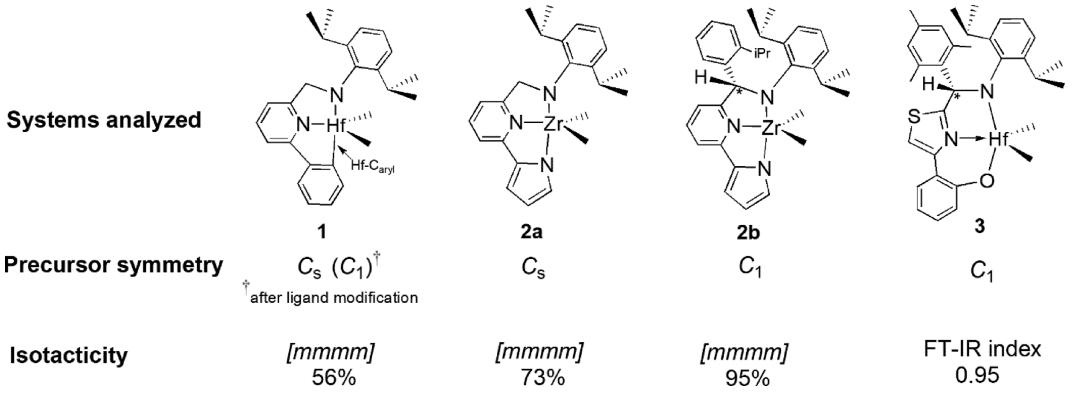

enlarge the toolbox available for inducing stereoselective olefin polymerization catalyzed by TM.

RESULTS AND DISCUSSION

First of all, we verified by DFT calculations the energetic differences (free energies) for the potential propene insertion in the M−X bond (M = Zr and X = N for systems **2a** and **2b**; M = Hf and X = O for system **3**) versus propene insertion in the M−CH_3 bond for systems **1**−**3**. The energetic differences of the low-lying transition states (TS) are called $\Delta E(\Delta G)_{C/X}$ and reported in Table 1 (second column). Negative values indicate that the first propene insertion generates a ligand modification before the further insertions in M-CH_3 bond (as system **1** in Chart 1). The (high) positive values of $\Delta E(\Delta G)_{C/X}$ we calculated for systems **2**−**3** (from 3.6 to 7.0 kcal/mol) suggest that the presence of heteroatoms in a place of C_{aryl} bond guides the first propene insertion to the M-CH_3 bond, so systems **2** and **3** are not suitable for in situ chemical ligand modification by monomer insertion (see Figure S3 for relevant TS geometries). Discarding this hypothesis, we investigated the stereoselectivity of propene insertion of system **2a** by using an ^{i}Bu residue to model the growing polymer chain. Interestingly, we found that the two low lying TSs for the two propene enantioface insertions are corresponding to structures with different coordination geometries. The insertion TS for the primary (or 1,2) *re* enantioface reported in Figure 1A, resembles a square pyramid (SP) whereas a distorted trigonal bipyramid (TBP) is obtained for the 1,2 *si* enantioface (Figure 1B). The (small) preference of TBP with respect to SP (see the $\Delta E(\Delta G)_{stereo}$ values reported in Table 1) seems due to a direct ligand−monomer effect: the *si* propene has the methyl group pointing toward the 2,6-^{i}Pr$_2$C$_6$H$_3$ ring and the way to alleviate the steric contact is by assuming a TBP coordination. In agreement with this hypothesis the preferred secondary (or 2,1) enantioface insertion is the one with a square pyramid structure and with the methyl group pointing far from the 2,6-^{i}Pr$_2$C$_6$H$_3$ moiety (see $\Delta E(\Delta G)_{regio}$ in Table 1 and Figure S4 for the TS geometries).

Table 1. Energetic Values (Free Energies) for the Propene TSs Calculated for Systems 1−3 of Chart 1[e]

system	$\Delta E(\Delta G)_{C/X}$[a]	$\Delta E(\Delta G)_{site1/2}$[b]	$\Delta E(\Delta G)_{stereo}$[c]	$\Delta E(\Delta G)_{regio}$[d]
1	−4.6 (−4.9)	6.1 (5.6)	0.7 (1.2)	2.0 (2.3)
2a	7.0 (7.8)	–	0.1 (0.3)	1.7 (0.7)
2b	4.9 (5.1)	0.4 (1.5)	2.6 (1.6)	1.1 (1.1)
3	3.6 (5.0)	2.2 (3.8)	2.1 (2.5)	3.5 (3.5)

[a]Calculated energetic preference for propene insertion on M−X versus M-CH_3 bond (X = C_{Aryl}, N and O for systems **1**, **2a**, **2b**, and **3**, respectively). [b]Energetic difference between propene TSs at site 1 (SP) and site 2 (TBP). Positive numbers indicate the energetic preference for site 1 with a SP structure. [c]Calculated stereoselectivity. [d]Calculated regioselectivity. [e]Values (in kcal/mol) are referred to the most stable TS set as reference point.

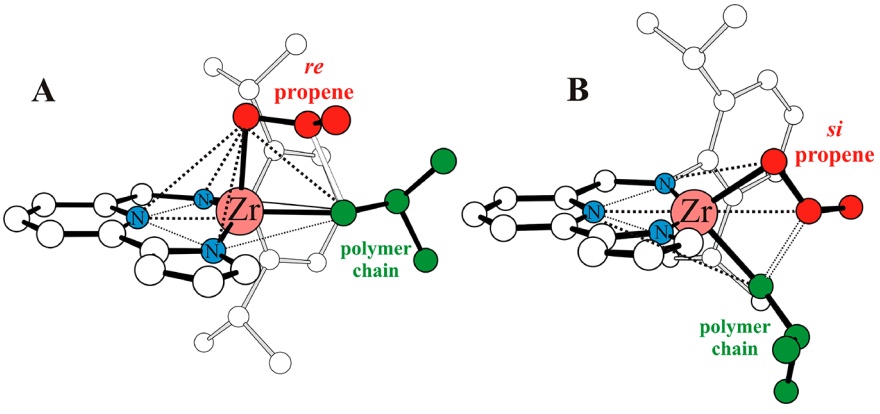

Figure 1. Propene insertion TSs into the growing polymer chain for the system **2a** with the *re* (A) and *si* (B) enantiofaces. The geometry resembles a square pyramid in structure A and a distorted trigonal bipyramid in structure B.

https://dx.doi.org/10.1021/acs.macromol.0c00280
Macromolecules XXXX, XXX, XXX−XXX

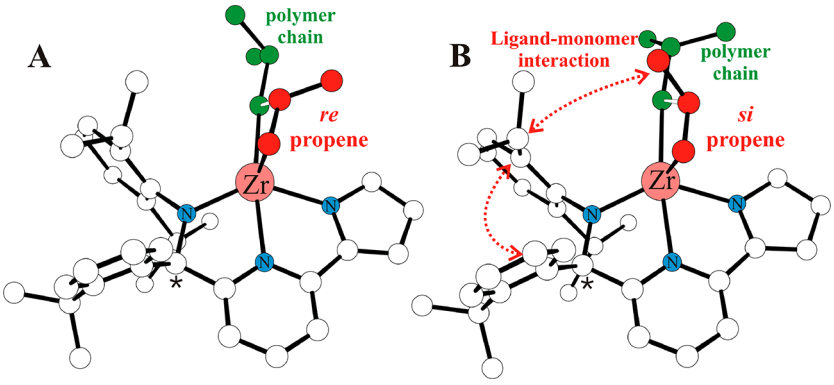

Figure 2. Propene insertion TSs into the polymer chain for the system **2b** with the *re* (A) and *si* (B) enantioface at the more stable site 1 with a SP geometry. The direct interaction of 2,6-$^{i}Pr_2C_6H_3$ ring with the *si* propene enantioface reinforced by the 2-isopropyl-phenyl substituent on the stereogenic C atom ∗ is shown by red arrows.

A way out to improve the stereoselectivity of the whole process by increasing the selection of propene enantioface may be moving from C_s to C_1 symmetry by adding a substituent on the methylene bridge bonded to the *N*-aryl ring so forming a stereogenic center (marked with ∗, compare systems **2a** and **2b** in Chart 1).[24] This generates an active species with two diasterotopic coordination sites analogously to the ones already discussed in literature for system **1** (and here called for simplicity site 1 for SP and site 2 for TBP).[16−18] Our results computed on systems **2b** and **3** (see Table 1) suggest that higher stereoselectivities are obtained via increasing the direct monomer interaction exerted by the 2,6-$^{i}Pr_2C_6H_3$ ring reinforced by the 2-isopropyl-phenyl substituent on the C* in a concerted mechanism (see Figure 2 for system **2b** and Figure S5 for system **3**) at the preferred active site 1 (see $\Delta E(\Delta G)_{stereo}$ and $\Delta E(\Delta G)_{site1/2}$ values reported in Table 1). This seems to correlate with the experimental finding of a higher isotacticity obtained by **2b** with respect to **2a** (see Chart 1).[24]

We call this "direct flow of information" to distinguish this chiral stereocontrol to the one reported for *ansa*-metallocene and postmetallocene systems based on the oriented growing chain that acts as "messenger of information between the chiral active site and the prochiral monomer".[20] It may help to recall at this stage that the results reported here are still not explaining the iPP produced by system **2a** because alternating propylene enantiofaces coming from enantiotopic sites should produce sPP (with low stereoregularity due to the small value of $\Delta E(\Delta G)_{stereo}$ of Table 1) and that is difficult to identify the driving force able to modify the migratory insertion step[27] (as **2a** and **3**, see the $\Delta E(\Delta G)_{site1/2}$ values of Table 1).[28] In order to find an explanation, we thought that a plausible modification of **2a** active sites geometry in solution may be obtained by additional coordination of chemical species at the metal center so inducing an octahedral environment similar to the one achieved by **1** after ligand modification in situ (see Figure S6A). Pellecchia and co-workers[23] stressed needing of Al$^{i}Bu_2H$ species in combination with methyaluminoxane (MAO) in order to obtain iPP with **2a** and suggested the formation homobinuclear/heterobinuclear equilibria, resulting in $[(N,N,N\text{-})Zr(\mu\text{-}H)nAl^{i}Bu_2]^{+}$ species[25] so we reinvestigated the propene polymerization of systems **2-3** in the presence of AlH−alkyl species.[29,30] For clarity we show the results obtained with $AlHMe_2$ after checking that they are really similar to the ones obtained with Al$^{i}Bu_2H$ species. We found a stable coordination of $AlHMe_2$ at the cationic active species **2a** (see $\Delta E(\Delta G)_{coord}$ column in Table 2)[31] with the formation of

Table 2. Energetic Values (Free Energies) for the Propene TSs Calculated for the Systems 1−3 of Chart 1 in the Presence of $AlHMe_2$[e]

system	$\Delta E(\Delta G)_{coord}$[a]	$\Delta E(\Delta G)_{site1/2}$[b]	$\Delta E(\Delta G)_{stereo}$[c]	$\Delta E(\Delta G)_{regio}$[d]
2a	−31.4 (−12.4)	−1.4 (−1.0)	2.0 (2.1)	2.3 (1.9)
2b	−34.0 (−13.5)	1.8 (2.7)	2.6 (2.7)	2.4 (2.5)
3	−38.0 (−16.5)	6.2 (6.5)	2.8 (3.0)	3.7 (4.0)

[a]Calculated energetic coordination of $AlHMe_2$ to the active species of Table 1.[31] [b]Energetic difference between propene TS insertions at site 1 (SP) and site 2 (TBP). Positive numbers indicate the energetic preference for site 1 with a SP structure. [c]Calculated stereoselectivity. [d]Calculated regioselectivity. [e]Values (in kcal/mol) are referred to the most stable TS set as reference point.

$N_{pyrrolic}$−Al bond and with the H bridge by Al and metal center (see Figure 3) whereas (much) lower $\Delta E(\Delta G)_{coord}$ are calculated by replacing $AlHMe_2$ with $AlMe_3$.[32] The final geometry shows a six-member ring resembling the seven-member ring obtained by **1** after monoinsertion product (for a direct comparison of the two systems, see Figure S6A and Figure S6B).

The additional effect of AlH−alkyl coordination to the TM center is to vary the energetics for the two available coordination positions for the monomer and growing chain (see Figure 3).[33] The preference we calculated for propene insertion TS reported in Figure 3B (having the growing chain trans to the coordinated Al species and a pseudo TBP geometry) with respect to analogous TS of Figure 3A (with the incoming monomer trans to the coordinated Al species and a SP geometry) is below 1 kcal/mol (see $\Delta E(\Delta G)_{site1/2}$ in Table 2) and molecular orbital analysis (MO) of the two TSs confirms the above statement (see Figure S7).[34] It is worthwhile to note that the preferred monomer enantiofaces for both sites *are the same* and are selected by a direct ligand control for the SP site (see Figure 3A) and by the chiral conformation of the growing polymer chain for the TBP site (Figure 3B). A further support of such assertion is obtained by analyzing the stereoselectivity of the propene insertion into $Zr-CH_3$ bond (so in the absence of a chiral polymer chain) and, accordingly, we calculated high stereoselectivities for the SP site and a lack of stereoselection for the TBP site.[35]

https://dx.doi.org/10.1021/acs.macromol.0c00280
Macromolecules XXXX, XXX, XXX−XXX

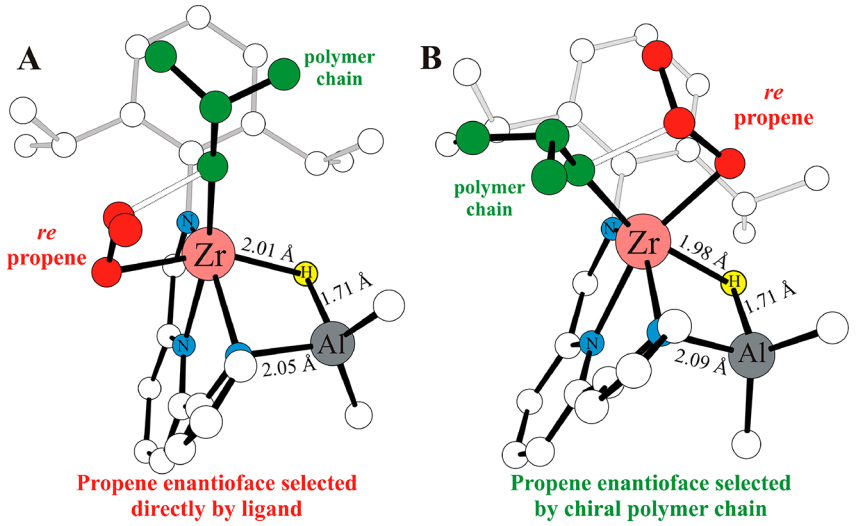

Figure 3. Propene insertion TSs into the polymer chain for system **2a** at the two diasterotopic active sites formed by $AlHMe_2$ coordination at the metal center. H atoms omitted for clarity with the exception of the one bonded to the metal (in yellow). Distances in Å.

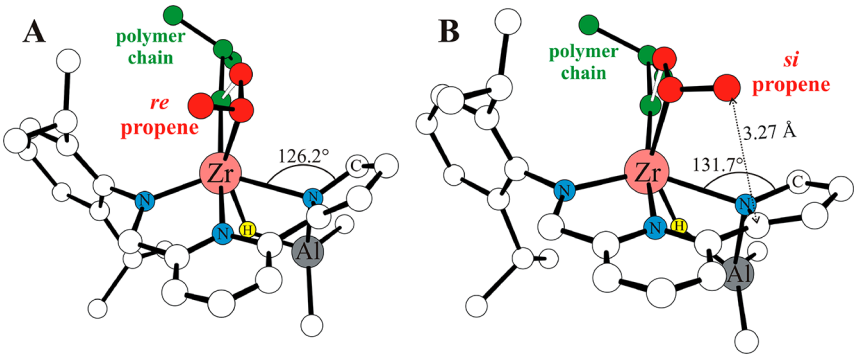

Figure 4. Secondary propene insertion TSs into the growing polymer chain for the system **2a** with *re* (A) and *si* (B) enantiofaces at active site 1 with $AlHMe_2$ coordination. The energetic preference of structure A with respect to structure B is 2.5 (2.4) kcal/mol and structure A shows the same enantioface of the preferred 1,2 insertion reported in Figure 3. H atoms omitted for clarity with the exception of the one bonded to the metal (in yellow). Distances in Å and angles in deg.

Two coordination sites of the same active species showing (different) origin of stereocontrol is unprecedented in TM-catalyzed polymerization; this may explain the isotactic control of **2a** and could also be exploited for enhancing the stereoselection of monomer insertion.

Direct experimental evidence of such active species has not been obtained by advanced 1D and 2D NMR spectroscopy experiments,[25] and we thought that a further support of our model may be found by computing the regiochemistry of propene insertion. The regiodefects detected in the ^{13}CNMR spectra of iPP samples synthesized with **2a** and **2b** show isolated regioinverted units with vicinal methyls in *threo* configuration attributed to the catalyst selection of the *same* propene enantioface for both 1,2 and 2,1 insertions.[23,36,37] In agreement with these experimental evidence we found that (1) the preferred 2,1 TSs are inserted at site 1 (see Figure 4) with a calculated value in line with the experiments (see $\Delta E(\Delta G)_{regio}$ of Table 2);[38] (2) the (high) preference (2.5 kcal/mol) for the 2,1 with *re* (Figure 4A) versus *si* enantioface is due to steric interaction of the latter with the pyrrolic moiety (see dotted line in Figure 4B) leading to a larger Zr−N−C angle of 131.7° with respect to 126.2°; (3) the preferred secondary insertion shows the same enantioface of the primary one (compare Figure 4A with Figure 3).

All these findings may be extended to the pentacoordinated C_1-systems **2b** and **3**;[39] for the former, both stereo- and regiocalculated values (see $\Delta E(\Delta G)_{stereo}$ and $\Delta E(\Delta G)_{regio}$ in Table 2) are higher with respect to **2a**, in agreement with the experimental data;[38] for the latter, the high value of $\Delta E(\Delta G)_{site1/2}$ reported in Table 2 indicates a polymerization stereocontrol with a clear preference for the direct monomer control similar to the one reported for the pyridylamido family (see Table 1).[16−18]

CONCLUSIONS

In conclusion, a theoretical analysis of propene polymerization promoted by pentacoordinated *N*-heteroarylpyridylamido tridentate ligands sorted out several catalyst design features: (i) these systems are prone to chemical modification with formation of active species showing coordination geometries different from the catalyst precursors; (ii) "Ewen's symmetry rules" reported in classical textbooks work well for *ansa*-metallocenes but should, at least, be updated to account for recent cases of active species modification;[40] (iii) the tacticity control by the chiral site can be exerted via a *direct ligand monomer interaction* and/or by *chiral conformation of the growing polymer chain*, and the competition of these two

https://dx.doi.org/10.1021/acs.macromol.0c00280
Macromolecules XXXX, XXX, XXX−XXX

models depends on a combination of electronic and steric factors.

■ ASSOCIATED CONTENT

Supporting Information

The Supporting Information is available free of charge on the ACS Publications Web site. The Supporting Information is available free of charge at https://pubs.acs.org/doi/10.1021/acs.macromol.0c00280.

Figures S1−S7 and computational details (PDF)

Cartesian coordinates of the structures discussed in the text (XYZ files) (ZIP)

■ AUTHOR INFORMATION

Corresponding Author

Giovanni Talarico − *Dipartimento di Scienze Chimiche, Università di Napoli Federico II, Via Cintia 80126, Napoli, Italy;* orcid.org/0000-0002-4861-0444; Email: giovanni.talarico@unina.it

Authors

Claudio De Rosa − *Dipartimento di Scienze Chimiche, Università di Napoli Federico II, Via Cintia 80126, Napoli, Italy;* orcid.org/0000-0002-5375-7475

Rocco Di Girolamo − *Dipartimento di Scienze Chimiche, Università di Napoli Federico II, Via Cintia 80126, Napoli, Italy;* orcid.org/0000-0001-8815-2997

Ana B. Muñoz-García − *Dipartimento di Fisica "Ettore Pancini", Università di Napoli Federico II, Via Cintia 80126, Napoli, Italy*

Michele Pavone − *Dipartimento di Scienze Chimiche, Università di Napoli Federico II, Via Cintia 80126, Napoli, Italy;* orcid.org/0000-0001-7549-631X

Complete contact information is available at: https://pubs.acs.org/10.1021/acs.macromol.0c00280

Author Contributions

The manuscript was written through contributions of all authors.

Notes

The authors declare no competing financial interest.

■ ACKNOWLEDGMENTS

We thank the University of Naples Federico II for funding (Ricerca di Ateneo 2017, DR_409_2017).

■ REFERENCES

(1) Stürzel, M.; Mihan, S.; Mülhaupt, R. From Multisite Polymerization Catalysis to Sustainable Materials and All-Polyolefin Composites. *Chem. Rev.* **2016**, *116*, 1398−1433.

(2) Baier, M. C.; Zuideveld, M. A.; Mecking, S. Post-Metallocenes in the Industrial Production of Polyolefins. *Angew. Chem., Int. Ed.* **2014**, *53*, 9722−9744.

(3) Talarico, G.; De Rosa, C.; Auriemma, F. Tacticity, Regio and Stereoregularity. *Polypropylene Handbook: Morphology, Blends and Composites* **2019**, 1−35.

(4) Busico, V.; Cipullo, R. Microstructure of Polypropylene. *Prog. Polym. Sci.* **2001**, *26*, 443−533.

(5) Ewen, J. A. Symmetry Rules and Reaction Mechanisms of Ziegler−Natta Catalysts. *J. Mol. Catal. A: Chem.* **1998**, *128*, 103−109.

(6) Kaminsky, W.; Külper, K.; Brintzinger, H. H.; Wild, F. R. W. P. Polymerization of Propene and Butene with a Chiral Zirconocene and Methylalumoxane as Cocatalyst. *Angew. Chem., Int. Ed. Engl.* **1985**, *24*, 507−508.

(7) Brintzinger, H.-H.; Fischer, D.; Mülhaupt, R.; Rieger, B.; Waymouth, R. M. Stereospecific Olefin Polymerization with Chiral Metallocene Catalysts. *Angew. Chem., Int. Ed. Engl.* **1995**, *34*, 1143−1170.

(8) Boussie, T. R.; Diamond, G. M.; Goh, C.; Hall, K. A.; LaPointe, A. M.; Leclerc, M. K.; Murphy, V.; Shoemaker, J. A. W.; Turner, H.; Rosen, R. K.; Stevens, J. C.; Alfano, F.; Busico, V.; Cipullo, R.; Talarico, G. Nonconventional Catalysts for Isotactic Propene Polymerization in Solution Developed by Using High-Throughput-Screening Technologies. *Angew. Chem., Int. Ed.* **2006**, *45*, 3278−3283.

(9) Arriola, D. J.; Carnahan, E. M.; Hustad, P. D.; Kuhlman, R. L.; Wenzel, T. T. Catalytic Production of Olefin Block Copolymers via Chain Shuttling Polymerization. *Science* **2006**, *312*, 714−719.

(10) Domski, G. J.; Lobkovsky, E. B.; Coates, G. W. Polymerization of α-Olefins with Pyridylamidohafnium Catalysts: Living Behavior and Unexpected Isoselectivity from a C_s-Symmetric Catalyst Precursor. *Macromolecules* **2007**, *40*, 3510−3513.

(11) Domski, G. J.; Edson, J. B.; Keresztes, I.; Lobkovsky, E. B.; Coates, G. W. Synthesis of a New Olefin Polymerization Catalyst Supported by an sp^3-C Donor *via* Insertion of a Ligand-Appended Alkene into the Hf−C Bond of a Neutral Pyridylamidohafnium Trimethyl Complex. *Chem. Commun.* **2008**, 6137−6139.

(12) Busico, V.; Cipullo, R.; Pellecchia, R.; Rongo, L.; Talarico, G.; Macchioni, A.; Zuccaccia, C.; Froese, R. D. J.; Hustad, P. D. Uni et Trini": In Situ Diversification of (Pyridylamide)hafnium(IV) Catalysts. *Macromolecules* **2009**, *42*, 4369−4373.

(13) Froese, R. D. J.; Hustad, P. D.; Kuhlman, R. L.; Wenzel, T. T. Mechanism of Activation of a Hafnium Pyridyl-Amide Olefin Polymerization Catalyst: Ligand Modification by Monomer. *J. Am. Chem. Soc.* **2007**, *129*, 7831−7840.

(14) Zuccaccia, C.; Macchioni, A.; Busico, V.; Cipullo, R.; Talarico, G.; Alfano, F.; Boone, H. W.; Frazier, K. A.; Hustad, P. D.; Stevens, J. C.; Vosejpka, P. C.; Abboud, K. A. Intra- and Intermolecular NMR Studies on the Activation of Arylcyclometallated Hafnium Pyridyl-Amido Olefin Polymerization Precatalysts. *J. Am. Chem. Soc.* **2008**, *130*, 10354−10368.

(15) Zuccaccia, C.; Busico, V.; Cipullo, R.; Talarico, G.; Froese, R. D. J.; Vosejpka, P. C.; Hustad, P. D.; Macchioni, A. On the First Insertion of Z-Olefins in Hafnium Pyridyl-Amido Polymerization Catalysts. *Organometallics* **2009**, *28*, 5445−5458.

(16) De Rosa, C.; Di Girolamo, R.; Talarico, G. Expanding the Origin of Stereocontrol in Propene Polymerization Catalysis. *ACS Catal.* **2016**, *6*, 3767−3770.

(17) De Rosa, C.; Di Girolamo, R.; Talarico, G. Chapter 8 - A General Model to Explain the Isoselectivity of Olefin Polymerization Catalysts. *Computational Quantum Chemistry* **2019**, 269−285.

(18) Domski, G. J.; Eagan, J. M.; De Rosa, C.; Di Girolamo, R.; LaPointe, A. M.; Lobkovsky, E. B.; Talarico, G.; Coates, G. W. Combined Experimental and Theoretical Approach for Living and Isoselective Propylene Polymerization. *ACS Catal.* **2017**, *7*, 6930−6937.

(19) Resconi, L.; Cavallo, L.; Fait, A.; Piemontesi, F. Selectivity in Propene Polymerization with Metallocene Catalysts. *Chem. Rev.* **2000**, *100*, 1253−1346.

(20) Corradini, P.; Guerra, G.; Cavallo, L. Do New Century Catalysts Unravel the Mechanism of Stereocontrol of Old Ziegler-Natta Catalysts? *Acc. Chem. Res.* **2004**, *37*, 231−241.

(21) Talarico, G.; Budzelaar, P. H. M. Analysis of Stereochemistry Control in Homogeneous Olefin Polymerization Catalysis. *Organometallics* **2014**, *33*, 5974−5982.

(22) Bahri-Laleh, N.; Hanifpour, A.; Mirmohammadi, S. A.; Poater, A.; Nekoomanesh-Haghighi, M.; Talarico, G.; Cavallo, L. Computational Modelling of Heterogeneous Ziegler-Natta Catalysts for Olefins Polymerization. *Prog. Polym. Sci.* **2018**, *84*, 89−114.

(23) Annunziata, L.; Pappalardo, D.; Tedesco, C.; Pellecchia, C. Isotactic-Specific Polymerization of Propene by a C_s-Symmetric Zirconium(IV) Complex Bearing a Dianionic Tridentate [-NNN-]

Amidomethylpyrrolidepyridine Ligand. *Macromolecules* **2009**, *42*, 5572−5578.
(24) Li, G.; Lamberti, M.; D'Amora, S.; Pellecchia, C. C_1-Symmetric Pentacoordinate Anilidopyridylpyrrolide Zirconium(IV) Complexes as Highly Isospecific Olefin Polymerization Catalysts. *Macromolecules* **2010**, *43*, 8887−8891.
(25) Li, G.; Zuccaccia, C.; Tedesco, C.; D'Auria, I.; Macchioni, A.; Pellecchia, C. NMR Spectroscopy and X-Ray Characterisation of Cationic N-Heteroaryl-Pyridylamido Zr^{IV} Complexes: A Further Level of Complexity for the Elusive Active Species of Pyridylamido Olefin Polymerisation Catalysts. *Chem. - Eur. J.* **2014**, *20*, 232−244.
(26) Diamond, G. M.; Hall, K. A.; LaPointe, A. M.; Leclerc, M. K.; Longmire, J.; Shoemaker, J. A. W.; Sun, P. High-Throughput Discovery and Optimization of Hafnium Heteroaryl-amido Catalysts for the Isospecific Polymerization of Propylene. *ACS Catal.* **2011**, *1*, 887−900.
(27) Cossee, P. Ziegler-Natta Catalysis I. Mechanism of Polymerization of α-olefins with Ziegler-Natta Catalysts. *J. Catal.* **1964**, *3*, 80−88.
(28) Roberts, J. A. S.; Chen, M.-C.; Seyam, A. M.; Li, L.; Zuccaccia, C.; Stahl, N. G.; Marks, T. J. Diverse Stereocontrol Effects Induced by Weakly Coordinating Anions. Stereospecific Olefin Polymerization Pathways at Archetypal C_s- and C_1-Symmetric Metallocenium Catalysts Using Mono- and Polynuclear Halo-perfluoroarylmetalates as Cocatalysts. *J. Am. Chem. Soc.* **2007**, *129*, 12713−12733.
(29) The noninnocent role of AlH^iBu_2 in polymerization in addition to the role of scavenger has been elucidated by Baldwin, S. M.; Bercaw, J. E.; Brintzinger, H. H. Cationic Alkylaluminum-Complexed Zirconocene Hydrides as Participants in Olefin Polymerization Catalysis. *J. Am. Chem. Soc.* **2010**, *132*, 13969−13971.
(30) Baldwin, S. M.; Bercaw, J. E.; Henling, L. M.; Day, M. W.; Brintzinger, H. H. Cationic Alkylaluminum-Complexed Zirconocene Hydrides: NMR-Spectroscopic Identification, Crystallographic Structure Determination, and Interconversion with Other Zirconocene Cations. *J. Am. Chem. Soc.* **2011**, *133*, 1805−1813.
(31) The dissociation energy (free energy) of $Al_2H_2Me_4$ is not included. For $Al_2H_2Me_4$, we calculated 32.1 (11.8) kcal/mol with the computational protocol reported in Supporting Information. The dissociation energy (free energy) of $Al_2H_2{}^iBu_4$ is 33.1 (15.6) kcal/mol with a $\Delta E(\Delta G)_{coord}$ of 34.1 (16.4) kcal/mol.
(32) The $\Delta E(\Delta G)_{coord}$ calculated for $AlMe_3$ coordination at the species **2a** is −16.6 (2.8) kcal/mol; these values are around 15 kcal/mol lower than the ones estimated for $AlHMe_2$ coordination (see Table 2).
(33) We verified that the formation of diasterotopic active sites may be obtained also by the coordination of $AlHMe_3^-$ at the cationic centre via -H bond, without the formation of $N_{pyrrolic}$-Al bond. However, in this case the active species is neutral.
(34) The MO analysis reported in Figure S7 shows that the HOMO energetic differences of TBP structure (Figure 3-B) with respect to SP (Figure 3-A) is 1.3 kcal/mol.
(35) For system **2a** the $\Delta E(\Delta G)_{stereo}$ for propene insertion into Zr-CH_3 bond at SP site is 2.3 (2.6) kcal/mol, very similar to the value reported in Table 2 for propene insertion in Zr-^{i}Bu chain; a (much) lower $\Delta E(\Delta G)_{stereo}$ of 0.2 (0.5) kcal/mol is calculated for analogous insertion at TBP site, in agreement with the chiral control of the growing polymer chain model.[20]
(36) Zhou, Z.; Stevens, J. C.; Klosin, J.; Kummerle, R.; Qiu, X.; Redwine, D.; Cong, R.; Taha, A.; Mason, J.; Winniford, B.; Chauvel, P.; Montanez, N. NMR Study of Isolated 2,1-Inverse Insertion in Isotactic Polypropylene. *Macromolecules* **2009**, *42*, 2291−2294.
(37) Paolucci, G.; Zanella, A.; Sperni, L.; Bertolasi, V.; Mazzeo, M.; Pellecchia, C. Tridentate [N, N, O] Schiff-base Group 4 Metal Complexes: Synthesis, Structural Characterization and Reactivity in Olefin Polymerization. *J. Mol. Catal. A: Chem.* **2006**, *258*, 275−283.
(38) System **2a** shows 73% of [*mmmm*] and around 3% of regioinverted unit in the propene polymerization whereas system **2b** show 95% of [*mmmm*] and 1.5% of regioinverted unit in the same experimental conditions (see reference 24).
(39) The coordination of AlH−alkyl species at systems **2b** and **3** may happen on the same (cis) or opposite (trans) side of the R substituents on the stereogenic chiral centre. In Table 2 we reported the more stable species due to the cis structures.
(40) A further example of modification of active species geometries with respect to the precursor ones has been reported for salalen-Ti systems showing a *fac-mer* coordination mode for the precursors; see Press, K.; Cohen, A.; Goldberg, I.; Venditto, V.; Mazzeo, M.; Kol, M. Salalen Titanium Complexes in the Highly Isospecific Polymerization of 1-Hexene and Propylene. *Angew. Chem.* **2011**, *123*, 3591−3594. However, calculations suggested a *fac-fac* wrapping mode for the active species; see. Talarico, G.; Budzelaar, P. H. M. Ligand Coordination Driven by Monomer and Polymer Chain: The Intriguing Case of Salalen−Ti Catalyst for Propene Polymerization. *Macromolecules* **2017**, *50*, 5332−5336.

https://dx.doi.org/10.1021/acs.macromol.0c00280
Macromolecules XXXX, XXX, XXX−XXX